REV.	BY & DATE	DESCRIPTION	CHECK	APPROVED & DATE
Prepared by B. A.	June 18, 2004	On-ground calibration report for the MAG instrument.		
B	Dec. 20, 2004	Time latencies in digital filtering corrected. Minor revision - re-routing for signature not deemed necessary.		

ADVISORY: This document has NOT been reviewed for export control and therefore may be subject to ITAR regulations or requirements

Ralph L. McNutt, Jr., Project Scientist and	Date: 6/24/04	Robert Gold, Payload Manager	Date: 6/21/04
Brian Anderson, Instrument Scientist	Date: 6/21/04	Mario Acuña, Cognizant Co-Invetigator	Date: 6/22/04
David Lohr, Instrument Engineer	Date: 6/21/04	Released	Date

PART NUMBER	SIZE	NEXT ASSEMBLY	QTY./NA	USED ON	EFFECTIVITY - END ITEM SER. NO.	WEIGHT

THE JOHNS HOPKINS UNIVERSITY
APPLIED PHYSICS LABORATORY
11100 JOHNS HOPKINS ROAD, LAUREL, MARYLAND 20723-6099

MESSENGER Magnetometer (MAG) Calibration Report

FSCM NO.	SIZE	DRAWING NO.	REV.
88898	A	7384-9464	B
SCALE NONE		DO NOT SCALE PRINT	SHEET 1 OF 22 ~~23~~

Table of Contents

INTRODUCTION

This document reports the calibration results for the MESSENGER Magnetometer (MAG) necessary for science analysis of the data returned by the instrument. The science objectives are described briefly to motivate the instrument performance characteristics, modes and calibration accuracy requirements. The instrument architecture and operations are described to provide background for the calibration activities, techniques and objectives. The calibration results provide verification of polarity for each axis, knowledge of the relative orientation of the three axes of the sensor, the telemetry to engineering conversion factors for each of the two instrument gain settings (ranges), the azimuth orientation of the sensor relative to spacecraft coordinates (about the Y spacecraft axis) which is the only orientation that cannot be determined precisely after launch and boom deployment, and determination of timing latency in the instrument. The spacecraft magnetics contamination requirements also flow from the science objectives and the steps taken to ensure compliance with these requirements are described together with a brief summary of the results demonstrating that these requirements are met. A detailed description of spacecraft magnetics mitigation techniques and assessment of the results for each sub-system are not necessary for science analysis from the Experimental Data Records (EDRs) and so are presented in separate reports.

SCIENCE OBJECTIVES

The primary science objective of the MAG instrument is to measure the structure of Mercury's magnetic field not only to determine the planetary magnetic moment, but more importantly to measure the structure of the planetary field both by constraining higher order moments and identifying crustal remanent fields. The Mariner 10 flyby observations indicate that the planetary moment is near 300 nT-R_m^3 [*Ness et al.*, 1976] (R_m is the planet's radius) although the uncertainties in the moment are large, about a factor of two, owing to the large contribution from external fields, primarily from magnetopause and magnetotail currents [*Connerney*, 1988]. Over the planet's pole the magnetic field is expected to be ~600 nT in magnitude and about 300 nT at the equator. The orbital coverage provided by the MESSENGER mission will allow determination of the planetary dipole moment to 10-20% without any correction for the external field [*Korth et al.*, 2004]. This improvement over the uncertainties in determinations from the Mariner 10 data is required to evaluate higher order structure in the field. At this level higher order structure in the field smaller than ~20% of the dipole strength could be attributed entirely to external field contributions.

Determination of higher order moments requires specification of and correction for the external magnetic field. Characterizing the structure of the magnetospheric field is therefore a necessary component of the science objective because it enables extraction of higher order moments of the intrinsic planetary magnetic field. Accurate specification of the external field can in principle allow determination of the intrinsic field to a precision of a few percent, roughly a factor of five to ten better than without an external field correction [*Korth et al.*, 2004]. Moreover, the statistical uncertainty in the inverted moment, including the effective noise contribution due to variable solar wind and interplanetary magnetic field (IMF) conditions at Mercury, allows unambiguous identification of quadrupole and octupole moments yielding contributions larger than ~2% of the dipole intensity at the surface. It is therefore necessary to measure Mercury's magnetic field to an accuracy of at least 2% of the planetary moment, that is, ~6 nT for the expected planetary moment.

There are several secondary science objectives which the magnetic field measurements address. These include: wave particle interactions both associated with field line resonances which should have periods comparable to ion gyroperiods (~ 1 to 7 Hz for protons) [*Glassmeier et al.*, 2003] and those associated with heavy ions in Mercury's exosphere that may play a role in the formation of the exosphere [*Potter and Morgan*, 1990]; magnetotail dynamics possibly analogous to substorms in Earth's magnetosphere [*Christon*, 1987]; magnetopause structure and dynamics for Mercury's small magnetosphere (compared both to the planet and to energetic ion gyroradii) under the solar wind conditions that generally prevail at Mercury [*Burlaga*, 2001] and which are very different from the average conditions prevailing at Earth and the outer planets; and characterization of field aligned currents linking the planet with the magnetosphere which are of great interest since they can provide insight into the interaction of a planet having no ionosphere with the magnetosphere/solar wind dynamo [*Slavin et al.*, 1997]. Wave amplitudes are expected to be near 1 nT, occasionally larger. Magnetopause turbulence is expected to be several nT in amplitude and extends up to and above ion gyrofrequencies (~2 Hz). Magnetotail dynamics has signatures of a few to 10s of nT and time scales of seconds to minutes. Field aligned currents may have signatures as small as a few nT or as large as 10s of nT and the regions of interest will be traversed in a few minutes.

DESIGN CONSIDERATIONS

The MESSENGER Magnetometer characteristics were determined primarily by the scientific objectives but also accommodate practical engineering constraints for integration and test and the need to conserve spacecraft telemetry. The dynamic range and resolution of the instrument are determined by the expected detectable structure of Mercury's magnetic field. Accounting for the effects of variability in the solar wind and interplanetary magnetic field at Mercury it should be possible to resolve higher order moments to about ~2% of an assumed equatorial surface field of 300 nT, or signals of about 6 nT [*Korth et al.*, 2004]. To support measurements over the range of expected fields at Mercury and conduct measurements during test and integration, MAG is equipped with two ranges: coarse, covering ±65,000 nT, and fine, covering ±2000 nT. An accuracy of 6 nT corresponds to 0.3% in the sensitive range. The accuracy objective imposes a requirement that the spacecraft magnetic field at the MAG sensor vary by less than ~ 1 nT and that the sensor orientation knowledge requirement be commensurate with 1% error (~600 nT maximum field) corresponding to 0.6 degrees. Detection of waves with amplitudes of 1 nT requires resolution below 1 nT, of the order of 0.1 nT at least. The MAG instrument provides 1.6 nT resolution in coarse range and 0.047 nT resolution in fine range and the gain factors were determined to an accuracy of 0.01% and 0.1% in coarse and fine range, respectively.

To meet the science objectives within mission telemetry constraints MAG accommodates a wide range of time sampling rates. At the minimum altitude of 200 km, the MESSENGER speed relative to the surface will be ~ 3 km/s, implying that a resolution comparable to roughly half the altitude is provided by a 30s sampling interval. However, characteristic time scales of Mercury's magnetosphere are much shorter, a few seconds, and wave particle interactions (the proton gyrofrequency at 500 nT is about 7.5 Hz) so sampling with a Nyquist frequency higher than a few Hz is strongly desired. The magnetic field data is also required to interpret data acquired by the MESSENGER Energetic Particle Spectrometer (EPS) which has a minimum sample interval of 5s. It is therefore strongly desired to have sampling of 1/s with options to sample faster than 10/s. During the mission cruise phase however, calibration of the spacecraft magnetic field and verification of polarity requires long term (many months) observations of the interplanetary magnetic field which can be accommodated using very low time resolution observations. Thus, there is also a need for very low sampling rates. MAG therefore uses selectable filter and sub-sampling techniques providing output sample rates from 20/s to 0.01/s.

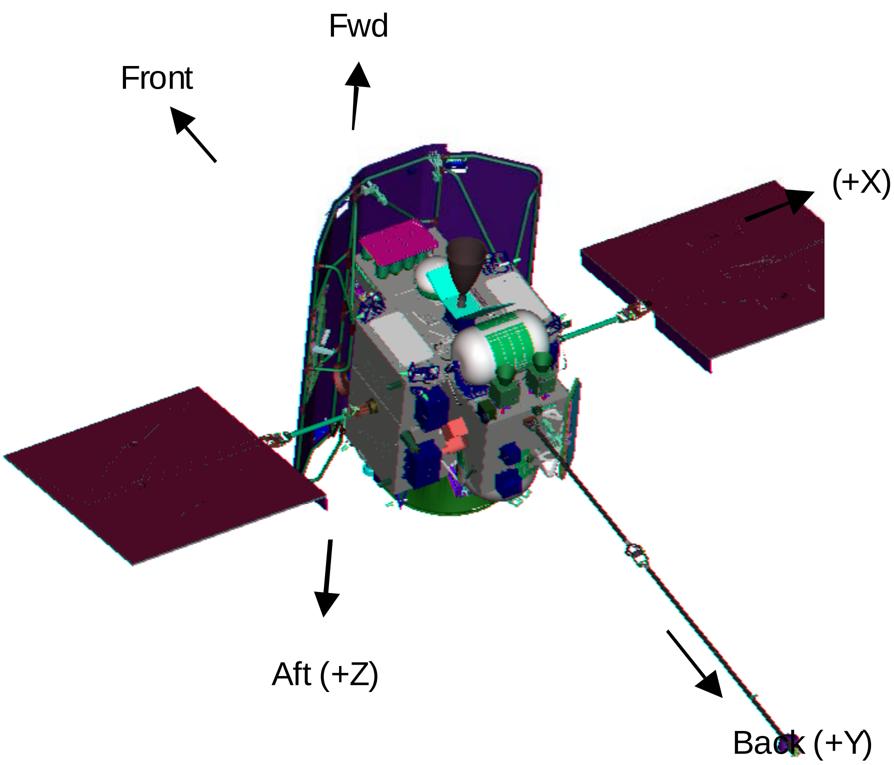

Figure 1. MESSENGER spacecraft showing the instrument coordinates and the magnetometer boom deployed in the +Y direction which is the anti-sunward direction during orbital operations.

To ensure that spacecraft fields at the MAG sensor are sufficiently stable to meet the science objectives, the MAG sensor is mounted on a boom that extends 3.6m from the spacecraft as shown in Figure 1 which also shows the spacecraft (SC) coordinate system. The boom extends in the +Y direction which is nominally anti-sunward during the mission's orbital phase. The payload adapter ring which also houses remote sensing instruments is on the +Z end of the spacecraft. The +X direction completes the right hand system. The MAG axes were chosen to correspond to the spacecraft system with only small corrections required to account for slight mounting uncertainties.

During orbital operations the spacecraft can be turned slightly so that +Y is not strictly anti-sunward. To protect the MAG sensor from direct exposure to solar illumination at Mercury, a small shade is included near the sensor. The shade frame is made of non-magnetic single alloy Titanium and the shade itself is a non-conducting ceramic fabric so this structure will not generate thermo-electric currents. Steps were also taken to ensure that the sensor and cabling could survive an unexpected attitude anomaly at Mercury that might place the boom and sensor in direct sunlight. All cabling was tested to ensure structural and electrical integrity were preserved on direct exposure to solar illumination at Mercury. Thermal balance tests of the blanketed sensor show that its temperature would remain below 150C, well below the temperature rating of all sensor components. During normal operations the sensor will be effectively cooled passively and is expected to be regulated by the sensor heater to stay at -15^{o}C. Instrument gain and offset stability for the sensor (determined principally by the core material which was characterized for previous missions, e.g. Voyager) are excellent yielding less than 0.25% change in gain over the entire range -40^{o}C to +50^{o}C and a change in offset of less than 2 nT in 50C^o. Use of room temperature calibrations therefore meets the science requirements for MESSENGER.

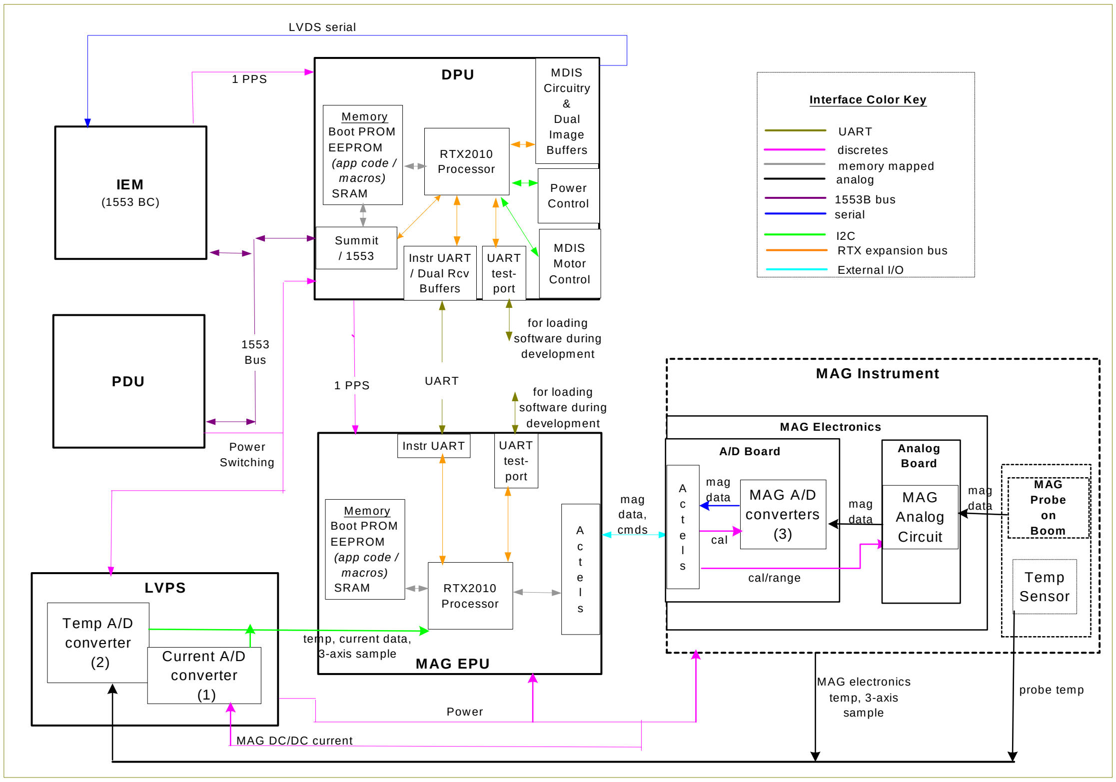

Figure 2. MESSENGER Magnetometer Instrument Block Diagram.

INSTRUMENT DESCRIPTION

The MESSENGER Magnetometer (MAG) is a three axis fluxgate magnetometer based on heritage from Near Earth Asteroid Rendezvous (NEAR), Advanced Composition Explorer (ACE) and Wind spacecraft. For MESSENGER, MAG employs somewhat miniaturized electronics to minimize mass resources. Essential instrument characteristics are summarized in Table 1 and a block diagram of the instrument and its electronic interfaces with the spacecraft is shown in Figure 2. The instrument consists of an electronics box and sensor. The electronics is mounted on the spacecraft and the sensor is mounted at the end of the boom. The electronics includes the fluxgate analog drive/sense circuitry for two gain states – fine and coarse, analog to digital conversion and associated programmable gate arrays, oscillator clock and dividers, experiment processing unit (EPU) including on-board memory, power converter, sensor survival heater drive with thermostatic control, and interface to the payload data processing unit (DPU). The mechanical and electrical interfaces between MAG and the spacecraft are described in the MAG-MESSENGER Interface Control Document: JHU/APL 7384-9223.

The analog outputs for the three axes are sampled simultaneously with three independent Sigma-Delta A/D converters at a rate of 20 conversions per second. The coarse and fine ranges have full scales (20-bit resolution) of 65,536 nT (0.063 nT) and 2048 nT (4 pT) respectively. The useful resolution is actually 18 bits and the intrinsic noise of the fluxgate sensor is ~10 pT. Instrument operation and modes are controlled and to a large extent implemented digitally in the on-board EPU. The functionality of the instrument is described in detail in the flight software specification document [MESSENGER Magnetometer Instrument Flight Software Specification: JHU/APL 7387-9041]. Briefly, the digitized 20-bit samples are digitally filtered to several low pass bands, 5 Hz, 2 Hz, 1 Hz or 0.5 Hz. The band used depends on the commanded output sample rate. The available rates are 20/s, 10/s, 5/s, 2/s, 1/s, 0.5/s, 0.2/s, 0.1/s, 0.05/s, 0.02/s and 0.01/s and allow the flexibility in operations required for the data volume constrained MESSENGER mission. For rates of 1/s and lower the data are sub-sampled from the 0.5 Hz filtered time series. The filtered data are then truncated to 16 bit values assembled into standard science packets of 200 samples each and forwarded to the DPU. By taking advantage of the fact that the most significant bits change infrequently, the software retains precision to the 17th bit of the internal 20-bit values by means of compression. In addition to these data, a 1 Hz to 10 Hz bandpass average amplitude is evaluated for any one of the axes, selected by command, and recorded as a log AC value with a 4-bit mantissa of the four most significant non-zero bits and a 4-bit power of two exponent of the 4th (least significant) bit of the mantissa. This is called the logAC value. It is created once per second and saved at that rate or at the commanded science rate, whichever is less frequent.

Table 1. MESSENGER Magnetometer essential characteristics.

Dimensions:	Sensor	8.1cm x 4.8cm x 4.6cm	
	Electronics	13.0cm x 10.4cm x 8.6cm	
	Boom	3.6 m long	
Mass:	Sensor:	184g	
	Electronics:	835g	
	Boom	2.66kg	
	Cable:	408g	
	Total:	4.09kg	
Power:	Instrument	4.2 W	
	Probe heater	0.93 W (2 W limited)	
Type:	Low noise tri-axial fluxgate (< 20 pT intrinsic noise level)		
A/D:	20-bit Sigma-Delta, 20 conversions/second		
	Self calibrating on command		
	Three independent units, one dedicated for each axis		
Ranges:	Coarse	±65,536 nT full scale	1.6 nT resolution (17 bits out)
	Fine	±2048 nT full scale	0.047 nT resolution (17 bits out)
Output Rates:	Maximum:	20/s (10 Hz analog filter) - internal A/D	
	Filtered:	10/s, 5/s, 2/s, 1/s (digital filter at Nyquist frequency)	
	Sub-sampled:	0.5/s, 0.2/s, 0.1/s, 0.05/s, 0.02/s, 0.01/s (0.5 Hz filter)	

In addition to the standard science packets three other types of data are generated: instrument housekeeping, instrument status, and burst. Instrument housekeeping consists of electronics and probe temperatures, low voltage power supply (LVPS) current, instrument state, command state, and fifty 3-axis magnetic field and logAC samples for every temperature, current and instrument/command state set reading. Instrument status data consists of instrument command counts, electronics and probe temperatures, LVPS current, and samples of the magnetic field as recorded by the 14-bit A/D converters which are integral to the LVPS. These LVPS A/D samples provide a back-up A/D conversion path with reduced precision in the unlikely event of a failure of one or more of the science A/D converters. Burst data consist of eight contiguous minutes of 20/s data. Burst collection is only allowed during a commanded time window when the logAC value exceeds a commandable trigger point and the instrument is in fine range. Burst mode will be used to allow sampling of large amplitude, higher frequency signals during parts of the orbit and mission phase when high rate sampling is not possible throughout the orbit due to telemetry volume constraints.

The instrument includes two internal calibrations. The first is an A/D calibration which is integral to the Sigma-Delta A/D converters and which adjusts the conversion scale against an internal voltage reference. The second is an analog calibration which injects a fixed current into the null current sensing amplifier and yields a fixed step function reference to monitor the long term stability of the analog amplifiers. The gains of the LVPS A/D converters are monitored relative to the Sigma-Delta science A/Ds via this analog calibration signal.

In time series and frequency domain analysis it is crucial that the observations be uniformly spaced in time. Moreover, since the MAG instrument uses on-board digital filtering it was essential that the sampling be uniform. For this reason the MAG samples are evenly spaced at 50 ms intervals driven by the oscillator internal to the MAG-EPU and are not synchronized to the spacecraft one second PPS. All three A/Ds are synchronized to the same sample trigger. The data are time tagged with the number of 50 ms ticks between the last PPS and the time that the A/D sample ready bit is set. Because the MAG-EPU clock and spacecraft clock will have some relative drift, the MAG time tag slips slowly relative to the spacecraft PPS resulting in an uncertainty of 25 ms in the precise time to which a given sample corresponds. The spacing between samples is however guaranteed to be uniform to within a microsecond.

The 25 ms maximum error in the absolute time is well within the timing needs for MESSENGER science since the timing accuracy requirements for MESSENGER are modest. The only other instrument with which MAG data will be correlated is EPS which has a minimum sample integration time of 5 seconds. At 25 ms, the uncertainty in knowledge of the spacecraft position for a given MAG sample is 75 meters, corresponding to a maximum relative velocity of 3 km/s relative to the planet at perigee. At the minimum altitude of 200 km this corresponds to an angular uncertainty relative to a point on the surface at nadir of 0.02^{o}, far smaller than the angular resolution to which the intrinsic field can be determined relative to external field sources [*Korth et al.*, 2004].

The A/D calibration is the single exception to strict even sampling. Every time this is done, four 50 ms samples are dropped, which is reflected in the MAG time tag. Because of the interruption of the data collection, A/D calibrations are only allowed between science data packets and are not allowed during bursts. An A/D calibration flag is set in the instrument housekeeping for the packet immediately following the A/D calibration. The digital filters are also re-set and require a few seconds to settle. For this reason, A/D calibrations are planned to occur only with the instrument in its highest sample rate (no digital filtering used) and at points of the orbit of least interest (highest altitude and in the solar wind).

CALIBRATION PROCEDURES AND RESULTS

The MAG calibration determines the following characteristics of the instrument and the MAG-spacecraft interface relevant to processing MAG data: (1) the absolute gain of the instrument in both ranges; (2) polarity of each axis, that is, the sign of the signal relative to physical direction of the field; (3) the relative orientation of the three sensor axes; (4) orientation of the sensor coordinates relative to spacecraft coordinates; (5) the internal fixed offsets for each axis in each range; (6) the spacecraft fixed magnetic field; and (7) the time latency between time tag assigned to each A/D conversion and the actual time to which the observation corresponds. The procedures and calibration results for each of these characteristics are presented in this section. For item (4), only the azimuth of the sensor about the Y axis needs to be determined in ground calibrations since the tilt/elevation of the sensor out of the spacecraft X-Z plane is best determined after boom deployment. The procedure for this in-flight orientation determination is also described here as are the methods for determining the fixed residual spacecraft magnetic field and verifying the polarity.

Coarse Range Absolute Calibration: Gain and Orientation

Absolute calibration was performed at the NASA Wallops magnetics facility. This facility consists of a set of 20-foot coils yielding a 3 foot diameter center zone with a field uniform to 0.005%, power control stability to better than 2 nT (verified to 0.5 nT during our tests) and alignment precision to < 0.01 degrees. An absolute scalar magnetometer with 1 nT absolute accuracy was used to specify the field used for this calibration. Figure 3 shows the MAG sensor held in a calibration fixture to control its orientation during these tests. Optical cubes on the fixture and on the end cap of the sensor provided precision alignment of the sensor using optical alignment equipment in the facility.

The technique used to provide absolute calibration and precise relative orientation of the three axes consisted of applying +50,000 nT (50,008 nT measured) in one direction and rotating the sensor in steps of approximately 45 degrees around each of the sensor's three axes. A total of 27 vector measurements were obtained (repeating the starting position for each axis). This procedure was repeated for a field of +10,000 nT (10,001.5 nT measured). Because the applied field is identical for each sensor orientation, the technique provides a precise correlation between both the gain and the orientation of the sensor axes. The gains and relative orientation are determined by using the fact that the magnitude is the same for all orientations. Denoting the counts in the X, Y and Z axes by c_x, c_y and c_z and the fixed offsets as c_{x0}, c_{y0} and c_{z0}, one writes the magnetic field in sensor coordinates as

$$
\begin{aligned}
B_x &= k_x(c_x - c_{x0}) \\
B_y &= \alpha k_x(c_x - c_{x0}) + k_y(c_y - c_{y0}) \\
B_z &= \beta k_x(c_x - c_{x0}) + \gamma k_y(c_y - c_{y0}) + k_z(c_z - c_{z0})
\end{aligned}
\qquad (1)
$$

where k_x, k_y and k_z are the gain coefficients for each axis and α, β, and γ measure the contributions of X in the Y axis (α), X in the Z axis (β), and Y in the Z axis (γ), respectively. Because the applied field, B_{appl}, is the same for all orientations of the sensor, the six parameters are constrained by the residual

$$\Delta^2 = \frac{1}{N}\sum_i \left(B_{x,i}{}^2 + B_{y,i}{}^2 + B_{z,i}{}^2\right) - B_{appl}{}^2 \qquad (2)$$

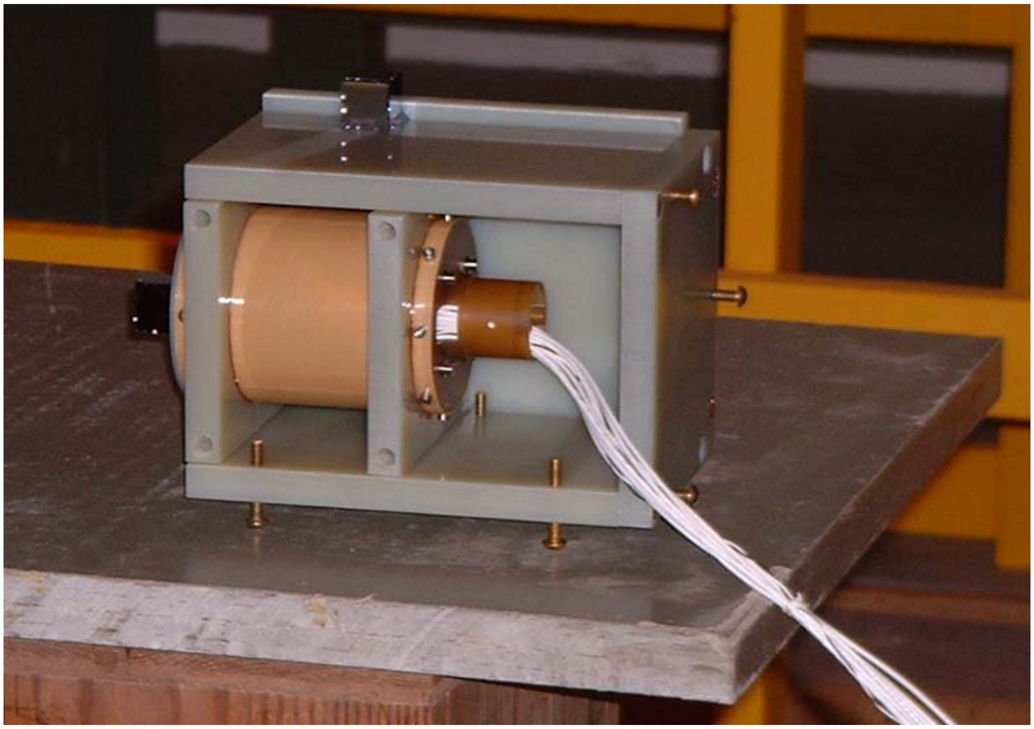

Figure 3. MESSENGER Magnetometer mounted in the calibration fixture placed in the center of the 20-foot coil facility at NASA Wallops.

Knowledge of the actual orientation at each step is not required since the solution only determines the relative orientation of the three axes. The offsets can either be treated as unknowns also constrained by equation (2) or measured. Equations (1) and (2) were solved by minimizing Δ^2 independently by GSFC and APL personnel using different code written in different languages. The GSFC approach used initial/preliminary measured offsets whereas they were allowed as free parameters in the APL solution. The two sets of inversion results are given in Table 2. Both the GSFC fixed offset and APL variable offset solutions had a very small residuals, Δ/B_{appl} = 0.008% for B_{appl} = 50,008 nT applied field and 0.014% for B_{appl} = 10,001.5 nT. The GSF solutions had slightly higher residuals (10% larger). The 50,008 nT case is considered the more accurate because the residual is only half as large as a percentage. This difference is attributed to having a larger applied field relative to variations in the field during the observations. Because the residuals for the APL values are slightly lower, we adopt the APL 50,008 nT values. The residual level and the excellent agreement between GSFC and APL results indicate that the coarse range calibration yielded gain results to 0.01% accuracy and relative orientation to 0.006^{o} (20 arc seconds). The geometry factors, α, β and γ apply to both ranges since they reflect the geometry of the sensor.

Table2. Inversions of equations (1) and (2) obtained independently by investigators at GSFC and APL.

	k_x	k_y	k_z	α	β	γ
GSFC: 50,008 nT	3.13002	3.12833	3.22095	-0.00461	0.00045	-0.00734
APL: 50,008 nT	**3.13026**	**3.12838**	**3.22058**	**-0.00462**	**0.00053**	**-0.00736**
GSFC: 10,001.5 nT	3.12937	3.12845	3.22298	-0.00477	0.00038	-0.00724
APL: 10,001.5 nT	3.12948	3.12833	3.22268	-0.00473	0.00036	-0.00729

Subsequent to these calibrations, the flight software was modified to accommodate 17-bit resolution in the telemetered data. The values given here are for 16-bit values. The values adopted are shown in bold. The k_x, k_y and k_z for 17-bit values are exactly ½ of the values given here.

Polarity Testing

The polarity of each axis was checked during instrument integration in two independent ways. The simplest and most reliable method uses the fact that the vertical component of Earth's magnetic field is downward in the northern hemisphere, in particular in Maryland and Virginia where all integration tests were done. By recording the sign of the signal from each axis as it is aligned with the vertical provides confirmation of the polarity. Alignment need only be within roughly 20^{o} of vertical for this to be definitive, so this test is easily done handling the instrument by hand. The second approach, used both at the Wallops and JHU/APL magnetics facilities, consists of approximately nulling the field at the coil center, placing the sensor in the coil center with its axes approximately aligned with the coil axes, applying a bias field of known direction along each of the three coil axes, and recording the polarity of the instrument signal. Aligning the sensor approximately, again within 20^{o} of the three coil axes is sufficient for this test. The second procedure also allows verification that the polarity of the two ranges is the same. The use of both techniques was used to ensure that any errors in the 'known' direction for the coil facilities would be identified. No errors in coil system polarities were found. For the initial testing both techniques showed that the X and Y sensor axes were opposite from that which would agree with nominal spacecraft coordinates with the boom deployed. When the sensor nulling coil leads were soldered for flight these axes were reversed and the correction of their polarity confirmed using both the Earth field comparison and the facility test at JHU/APL.

A final polarity test was performed after instrument integration to the boom and the spacecraft. This was done using a test magnet whose North magnetic pole was known (determined by comparison of the Earth field polarity test and a field test magnetometer). By aligning the test magnet so that its N-S axis was approximately aligned with one of the MAG axes and orienting the test magnet so that the S pole is closest to the MAG the field along the axis of the test magnet points from the MAG sensor to the test magnet. Reversing the orientation of the test magnet reverses the polarity of the field along the MAG-sensor/test magnet line. Using this procedure the polarity of the MAG sensor as integrated with the boom and the spacecraft was confirmed to be as designed, that is, such that it will correspond nominally (to within mounting accuracies) to spacecraft coordinates following boom deployment.

Two post launch polarity confirmations will be performed either of which is sufficient. In the first, long term measurements of the interplanetary magnetic field will be compared with independent measurements at other spacecraft such as ACE or Wind. The IMF is well ordered by its sector structure which follows the solar rotation and the solar wind flow so that it is straightforward to line up the sector polarity measured by ACE or Wind near 1 AU at Earth and that at MESSENGER. This polarity test best determines the components in the ecliptic plane. The polarity of the out of ecliptic plane is then readily determined by spacecraft roll maneuvers which will be done to determine spacecraft residual fields and sensor elevation orientation relative to the spacecraft X-Z plane (see below). The second polarity check is provided by the Earth fly-by observations by comparing the measured field with the Earth's known field. The Earth field comparison is primarily being done as an independent test of sensor orientation and the polarity confirmation occurs in order to perform the orientation verification and is essentially identical to that performed for the NEAR magnetometer [*Anderson et al.*, 2001].

Azimuth Orientation

The relative orientation of the sensor and the optical cube on the sensor housing end cap was determined at the Wallops magnetics test facility as follows. The sensor was oriented with the Y axis (the axis of the cylindrical housing) parallel to one horizontal axis of the facility by reflecting a laser off of the optical cube on the end cap. The sensor was then rotated about the Y axis to exactly reflect the laser to the source and the alignment of the laser relative to the horizontal measured using the optical equipment of the facility. The accuracy of both alignments was limited by the size of the laser spot and corresponds to 0.04^{o}. A vertical field was then applied and the X and Z magnetic field readings recorded. The ratio of X and Z fields then yields the angle of the sensor axes relative to vertical (or horizontal). The cube was found to be rotated 2.4^{o} clockwise (right handed) viewed looking toward the +Y side of the spacecraft (i.e. toward the spacecraft from the magnetometer) relative to the X-Z sensor directions. After integration to the boom and with the boom deployed (vertically) the end cap was measured to be rotated 2.0^{o} clockwise (right handed) viewed looking toward the +Y side of the spacecraft relative to the root hinge optical cube. The root hinge cube in turn was found to be rotated 0.5^{o} also clockwise (right handed) viewed looking toward the +Y side of the spacecraft. Thus, the X-Z spacecraft axes are rotated 0.1^{o} clockwise (right handed) looking toward the +Y side of the spacecraft relative to the X-Z magnetometer sensor axes. The conversion of the X and Z components from sensor to spacecraft coordinates is therefore a 0.1^{o} rotation as shown in Figure 4.

The conversion for this azimuth orientation to spacecraft from magnetic sensor coordinates is

$$
\begin{aligned}
B_{x-sc} &= 1.0000 B_{x-mag} + 0.0017 B_{z-mag} \\
B_{z-sc} &= -0.0017 B_{x-mag} + 1.0000 B_{z-mag}
\end{aligned}
\qquad (3)
$$

This conversion only accounts for the pre-flight azimuth conversion. The final orientation conversion from sensor to spacecraft coordinates will be determined after launch as described below.

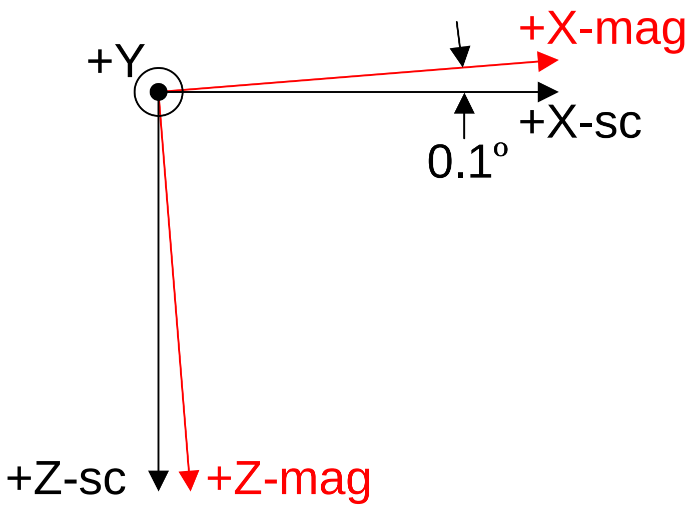

Figure 4. Relative azimuth orientation of magnetic sensor (mag) and spacecraft (sc) coordinates determined from alignment and magnetics calibration measurements.

Elevation Orientation: In-flight Technique

The elevation orientation is defined as the direction of the normal to the sensor X-Z plane relative to the normal to the spacecraft X-Z plane. Since this angle depends on the equilibrium points of both boom hinges, which in turn are likely to be slightly different in space than in ground testing, the elevation orientation is difficult to determine in pre-launch tests. In fact however, this orientation is very accurately determined in-flight by taking magnetic field measurements while the spacecraft rolls about the Y axis. The ambient field appears to rotate in the sensor frame of reference while any spacecraft or residual instrument offset field appears as a fixed field. The rotating field appears primarily in the X and Z axes but some amplitude will generally appear in the Y axis. The amplitude of the roll signal in the Y axis relative to that in the X-Z plane gives the tangent of the angle between the sensor X-Z plane normal and the spacecraft X-Z plane normal. In addition, the phase of the Y roll signal relative to the X axis roll signal gives the azimuth of the sensor X-Z plane normal about the spacecraft Y axis. This technique has been used in interplanetary space on numerous missions including Voyager and NEAR and typically yields the sensor X-Z plane normal direction to accuracies of 0.1^{o}, more than adequate for MESSENGER requirements. (On spinning spacecraft such as ACE, it must be accurately determined to properly de-spin the magnetic field observations.) The same observations also provide accurate determination of the X and Z components of the residual fixed magnetic field at the sensor. This residual magnetic field is expected to be < 1 nT but is not measured prior to launch. The Y component of the residual fixed field is not determined by this technique.

The Earth fly-by which is afforded by the July-August 2004 launch scenario provides the only post-launch opportunity to verify the azimuth orientation. It also provides an independent confirmation of the elevation orientation. Comparison with Earth field during fly-by encounters provides orientation accurate to 0.1° by comparing the measured vector field to well known Earth model fields and has been done previously by the MAG investigators [*Anderson et al.*, 2001].

Fine Range Gain Calibration

The fine range gain factors were determined by measuring the fine range response relative to the coarse range using the 2-meter coil system at JHU/APL. The APL magnetics facility provides a 2-foot diameter zone in which the field is uniform to 0.01%. The current control system is linear to 0.01% and provides 1-2 nT stability. The absolute accuracy is about 0.5% so this facility was not used for absolute calibration. With the sensor in the coils operating to approximately null the background field, a series of currents were applied to the facility coils to determine the response per unit coil current in coarse range. The range was then set to fine and another series of smaller currents were used to determine the signal response per unit coil current in fine range. This was repeated for each sensor axis (the vertical coils were used for each axis so the sensor was re-oriented to cross-calibrate each axis). The measured ratios of the scale factors between the two ranges are given in Table 3. The uncertainties are determined from the 1-sigma uncertainties in the slope determinations for the coarse and fine response per unit system coil current. The fine scale calibrations are accurate to 0.08% or better.

Table 3. Relative scaling factors between fine and coarse ranges.

Axis	k_{fine}/k_{coarse}	÷32	Uncertainty (%)
X	33.465	1.04578	0.03
Y	33.514	1.04731	0.07
Z	33.550	1.04844	0.08

MAG Internal Offset Determination

The instrument offset was determined four different ways and the results are shown in Table 4. The first method, called the Wallops flip, consisted of flipping the sensor during the Wallops calibration. A small field was established in the facility and the sensor was then rotated 180° and back to an accuracy of 5°. The response of the two components in the plane of rotation was recorded for both orientations. Since the instrument offset rotates with the sensor, the average of the output for the two orientations gives the offset. The precision of the 180° rotation is not critical since even a 5° error only introduces a 0.4% error in the offset. This flip technique is the most direct means of measuring the offset but it requires a steady uniform field. The Wallops flip measurement is considered more reliable than the other flip measurements.

Flip offset measurements were also made at the APL magnetics facility and with the sensor at the bottom of a mu-metal can to verify consistency before and after environmental testing and to establish the correspondence between coarse and fine ranges. For the 'Can flip' a set of three layer cans at JHU/APL, used for instrument bench level testing, and were also used for the offset measurements. Demagnetizing the cans yields a residual field less than a few nT. Uncertainties in the can flip measurements arise from possible non-uniform residual fields in the can, moving equipment (chairs, elevators etc.) and the precision to which one can rotate the sensor. The APL flip was done as at Wallops but in the APL magnetics facility. Since the field is less uniform than at Wallops the test is considered less accurate. The three tests gave comparable results. Moreover, the can flip tests show that

that the fine range and coarse range offsets scale almost precisely with the gain factors. The offsets from each technique were used in the calibration inversion based on the Wallops scale factor calibration data. The residuals of these inversions in nT are given in the right hand column of Table 4. The Wallops flip inversion gives the lowest residual consistent with the expected relative accuracy of the techniques.

The fourth method of determining the offsets consists in allowing the offsets to be free parameters in the inversion using equations (1) and (2). The results of this inversion are shown in the row of Table 4 labeled ‘Wallops Inversion’ and gave the lowest residual, 4 nT. These offsets are the same as those obtained in the Wallops flip – the difference in the residuals, 4.0 vs 4.4 nT is not considered significant and is due to slightly different values for the other coefficients given by the two inversions. We adopt the Wallops flip values for the instrument offsets. The other tests give results basically consistent with these results. The can flip tests for the fine range show that the offset is essentially identical in nT between the two ranges so the fine range offsets are obtained by scaling the Wallops flip results for the coarse range using the relative range scale factors (Table 3). The adopted fine range offsets are given in the bottom row of Table 4.

Table 4. Internal instrument offsets

Test	Range	X-axis	Y-axis	Z-axis	Res. (nT)
		16-bit counts (nT equivalent)			
Wallops Flip	Coarse	**-15.2 (-48)**	**-32.6 (-102)**	**-8.1 (-26)**	4.4
Cans Flip	Coarse	-17.0 (-52)	-39.0 (-120)	-19.0 (-55)	19.2
Cans Flip (fine)	Fine	-520 (-51)	-1197 (-117)	-547 (-57)	N/A
APL Flip	Coarse	-11.2 (-35)	-26.6 (-83)	-7.2 (-23)	10.4
Wallops Inversion	Coarse	**-15.2 (-48)**	**-32.6 (-102)**	**-8.1 (-26)**	4.0
Wallops (scaled)	Fine	**-509 (-48)**	**-1093 (-102)**	**-272 (-26)**	N/A

NOTE: Internal instrument offsets in 16-bit resolution counts and their equivalent in nT for the four offset measurements. The values adopted are shown in bold. Note that 17-bit offset counts are twice the values given here.

Spacecraft Fixed Residual Field Determination

The science objectives for MAG require that the spacecraft residual field be constant to within 1 nT. Since this is not a mission to measure the interplanetary magnetic field (IMF) we use the known properties of the IMF to provide calibration of the spacecraft residual field. This is done in two ways. First, spacecraft maneuvers allow separation of the ambient field from sources that are fixed with respect to the spacecraft. The roll maneuver discussed above provides the X and Z components of the residual spacecraft field. Measurement of the Y component using spacecraft maneuvers requires a rotation about either the X or Z spacecraft axis and is called a flip maneuver because it flips the front and back sides of the spacecraft relative to the spacecraft-Sun direction. These maneuvers are not generally possible due to Sun illumination constraints of other instruments. For thermal and power management reasons a few spacecraft flips are planned and the magnetometer is planned to be operating during these events to provide calibration opportunities for the Y component residual field. Other half-flip maneuvers are also possible, in which the spacecraft tips up and down about the X axis by 90^o, giving a near 180^o swing without violating instrument illumination constraints. The data from these flips only provide 180^o

rotation rather than multiple complete revolutions given by the roll maneuver. The determination of the Y residual field will therefore be less accurate.

The known properties of the IMF will therefore be used to complete the Y component residual field determination. On time scales of hours and days, variations in the IMF are predominantly rotational. This being the case, the natural fluctuations can be used to identify the zero point of the field by identifying a fixed vector offset in the measurement which yields a field that is on average orthogonal to the fluctuations. Moreover, on month and year time scales, the vector average of the IMF tends to zero. Thus, using long term continuous observations, one can use the rotational characteristics of the IMF to identify the 'zero' point of the IMF which in turn is the vector residual field of the spacecraft. Combining these determinations with the X and Z residual determinations from the rolls and the Y residual estimates from the flips allows a robust determination of the spacecraft vector residual field. Analysis identical to this approach used on Voyager, ACE (spin axis) and NEAR gave residual field determinations accurate to < 1 nT, sufficient for MESSENGER science requirements [e.g. *Anderson et al.*, 2001]. The low rate, 0.01/s sampling, will be instrumental in conducting the required long term IMF observations to support this analysis without burdening spacecraft operations.

Timing Latencies

The MAG samples are time tagged to 0.05 s using an internal clock that counts the number of 0.05 s intervals since the last time pulse, PPS, from the spacecraft DPU. On average the time tag is therefore 0.025 s behind since if a square-wave jump occurs any time two A/D conversions, i.e. between $t = t_{last}$, and $t = t_{last} + 0.05$ s, it is tagged no sooner than $t_{last} + 0.05$ s. Other fixed latencies are introduced by the characteristic response time of the fluxgate and by the anti-alias filtering before and in the Sigma-Delta A/D converters. The combined latency was measured as follows. In the engineering unit the PPS signal was accessible and was used to trigger a 0.5 second long square pulse in a signal generator. The signal generator sourced a current to a test coil positioned in the shielding can with the MAG sensor. The inductive time constant for the test coil was less than 1ms. The first differences of the instrument output signal were then calculated, that is, $dB_i = B_i – B_{i-1}$ and assigned the average time, $t_{dB,i} = (t_i + t_{i-1})$. Over a period of hours, the DPU clock and the MAG EPU clock drift by more than 50 ms so accumulating dB_i, $t_{dB,i}$ pairs over several hours provides a statistical sample of the appearance of the leading edge of the square pulse in the MAG data. Figure 5 shows this data relative to even seconds in the MAG telemetry. If there were no instrument latency all of the points would appear at $t_{dB} = 0.025$ s, but more than half of the dB_is appear at 0.075 s and a fraction at 0.125 s. The average $t_{dB,i}$ weighted by $|dB_i|$ gives the total latency. This is 0.067 s or an additional 0.042 s over the 0.025 s from the time tagging. The average true time of the magnetic field samples is therefore obtained by subtracting 0.067 s from the time tag given in the MAG telemetry.

The expected instrument latency is in excellent agreement with the measured value of 42 ms. The anti-alias filtering (15.9 ms time constant) and the instrument feedback response (time constant of 3.2 ms) in series account for 16.3 ms. The A/D conversion time is 49.5 ms corresponding to a latency of 24.8 ms. The expected instrument latency is the sum of 16.3 ms and 24.8 ms or 41 ms.

Digital filtering introduces additional latency relative to the 20/s data. The digital filters are Butterworth IIR filters with their 3 dB points set at the Nyquist of the sampling rate (e.g. 0.5 Hz for 1/s sampling or rate #6) as shown in Table 5. Rates 0 through 6 are sub-sampled from the 0.5/Hz filtered time series and all have the same time lag. Rates 7, 8 and 9 have different digital IIR filters and correspondingly different lag times. Rate 10 is not digitally filtered and is lagged by 42 ms.

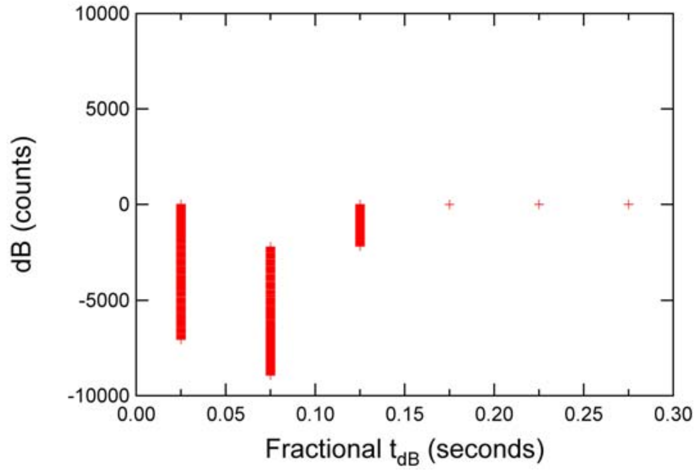

Figure 5. First point differences versus fractional time delay response for a 1 PPS triggered input square pulse magnetic field. All of the first point differences would appear at 0.025s in the absence of any additional latencies in the instrument.

Rate	Samples/sec	IIR 3dB (Hz)	IIR Lag (sec)	Net Lag (sec)
0	0.01	0.5	2.316	2.358
1	0.02	"	"	"
2	0.05	"	"	"
3	0.10	"	"	"
4	0.20	"	"	"
5	0.50	"	"	"
6	1.00	"	"	"
7	2.0	1.0	1.144	1.186
8	5.0	2.5	0.435	0.477
9	10.0	5.0	0.181	0.223
10	20.0	N/A	0.0	0.042

Table 5. MESSENGER Magnetometer sample rates, digital IIR filter 3 dB points, IIR time lags and net time lags.

The time lags are given by the properties of the digital filters and were confirmed in testing as follows. A triangle wave from a signal generator was used to drive a coil to generate a triangle wave magnetic field signal and data were obtained both in the desired commanded rate (5, 6, 7, 8, 9 and 10) simultaneously with a high rate (rate 10) eight minute burst sample interval. Since the burst channel data is taken at the native 20/s rate comparison of these data against the commanded science data allows direct confirmation of the lag introduced by the digital filter. The time lag between the commanded science rate data and the burst data was evaluated by constructing the mean square residual between the science channel data and the burst channel data interpolated to the lagged science data sample time as a function of the lag time. A parabola was then fit to this function and the minimum of the parabola gives the time lag. Figure 6 shows the two time series and the residual time lag result for the rate 6/burst comparison. The lags obtained in this way were accurate to 1 ms (3-sigma) and agreed with the theoretical values and are given in Table 5. The net time lag including both the instrument and digital filter time lags are given in Table 5. The physical sample times are obtained by subtracting the net lag from the time tags reported in telemetry.

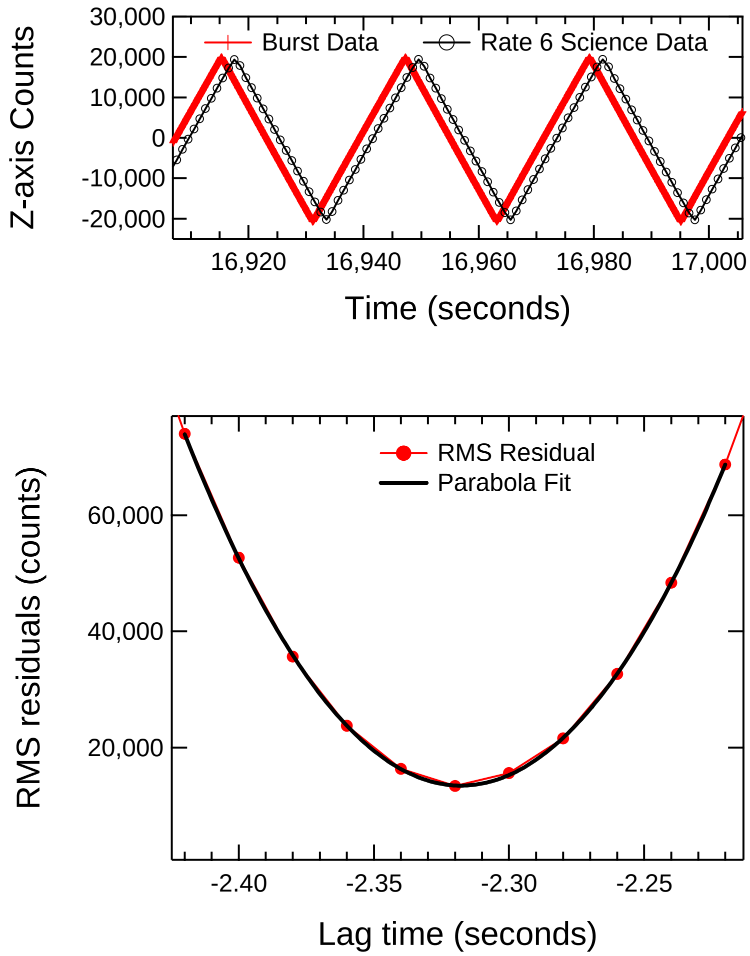

Figure 6. Digital filter time delay confirmation in ground testing. Top panel shows burst and science channel data obtained in ground testing for a triangle wave field showing the time delay between the filtered rate 6 science channel data and the unfiltered burst channel data. Bottom panel shows the mean square residual between the burst and science data versus lag time.

.

Spacecraft Magnetics Summary

All components of the spacecraft employing magnets or magnetic materials were screened for magnetic signatures. In addition, current loops in large current systems were avoided in the design of the battery, solar arrays, power distribution system and spacecraft harness. The three spacecraft systems that employed magnets or magnetic materials presenting the greatest risk to the magnetometer were, in decreasing order of significance, the propulsion latch valves, the momentum reaction wheels, and the battery cells. The steps used to mitigate these sources of contamination are summarized in this section.

The magnetic moment of each latch valve of the propulsion system was characterized prior to assembly of the propulsion system to 1% accuracy at the JHU/APL magnetics facility. The geometry of the propulsion system was then used to construct a mathematical model of the propulsion system field and estimate the field at the deployed magnetometer location. This model was tested against measurements of the magnetic field of sub-assemblies of the propulsion system and found to be consistent with the measurements to within the ~20% noise level of the measurements (due to the magnetic contamination of a conventional work area at the propulsion system vendor). This level of accuracy is more than sufficient to demonstrate that the model was free of gross errors (e.g. sign errors). A pair of cancellation magnets was then designed to cancel the propulsion system field at the deployed sensor location. The cancellation magnets were attached to the spacecraft structure early in integration.

The momentum wheels were tested at the vendor site for magnetic signatures and found to yield signals larger than 0.3 nT at the deployed sensor location. The source was identified as a magnetic moment rotating with the momentum wheel. Steps were therefore taken to minimize the magnetic signatures of the wheels. A subsequent visit to the vendor confirmed that the rotors were the source of the magnetic field and that demagnetizing the rotors and rotor bearings reduced the magnetic signature by a factor of three. Tests with metglass shielding showed that an additional factor of three could be obtained using a single layer of 0.4 mil thickness material. A test shield was fashioned and brought to the vendor to verify that the shielded flight wheels met the variable magnetic field contamination goal of < 0.03 nT at a distance of 4 meters. All wheels passed this test and magnetic shields were fashioned for all four wheels and installed on the spacecraft. The shielding mass for each wheel was 33 g. Tests during integration confirmed that the magnetic field from the wheels was less than 10 nT at distances from the wheels of less than 20 cm. (The shields could not be installed until after testing was completed that used magnetic signatures of the wheel rotation to confirmation of the sense of wheel rotation as indicated by the attitude control system.)

The battery cells use Nickel in both the casing and in the active elements of the battery. The cells were demagnetized using a solenoid degausser in an ambient field less than 0.5% of Earth's field at the JHU/APL magnetics facility. This reduced the residual magnetic moment of the cells by roughly a factor of ten from their moments as delivered from the manufacturer. Numerous other spacecraft components were demagnetized to minimize their contribution to any spacecraft residual field. These included: stainless steel hardware required for the phased array antenna, solar array interconnects (after delivery of the solar arrays using a hand demagnetizer) and stainless steel 'velcro' fastening material for the spacecraft sunshade.

The fixed residual spacecraft moment of the spacecraft was assessed near the end of spacecraft integration by means of a pendulum test in which the spacecraft was suspended from an overhead crane, displaced 2 feet horizontally from vertical at the payload adapter fitting (bottom) by pulling laterally at the bottom of the spacecraft. Releasing the spacecraft provided a clean pendulum motion without stressing the spacecraft structure. The magnetic signature of the spacecraft was monitored simultaneously by three test magnetometers. This test confirmed that there were no magnetic field sources other than those identified above: the only detectable sources were due to the combination of the propulsion valves and compensation magnets, consistent with the net field expected from the magnetic field model developed for the propulsion system modified to include the cancellation magnets.

Variable spacecraft fields were monitored by operating the flight magnetometer in its stowed configuration while spacecraft systems were tested. To maximize the sensitivity of these tests, a set of three coils were constructed and placed near the magnetometer to allow approximate cancellation of the Earth's field to allow operation in the fine range. Figure 7 shows this configuration as used during a Comprehensive Performance Test (CPT) at JHU/APL during final integration. No signals associated with the momentum wheels were detected at a level of 1-2 nT. Additional 'sniffing' measurements with a test magnetometer of the reaction wheels, power distribution system, solar array drive motors, and other systems revealed no magnetic signatures at a level of 10 nT at a distance of ~ 20 cm, consistent with a field at 3.6 meters of less than 2 pT. The only signal identified in the stowed flight magnetometer data was a 10 nT step associated with a propulsion tank heater within 20 to 40 cm of the flight sensor as stowed. This corresponds to a field of less than 0.02 nT at the deployed MAG sensor. Of particular interest was the fact that no signal was detected when the battery changed from a charging state to a discharge state. The batter layout was designed in a figure eight current path configuration and tested to ensure that the magnetic field created by the current flow in the battery was a quadrupole. The CPT measurements confirm that this design was successful.

Figure 7. Coils used to cancel Earth field allowing flight MAG measurements in fine range during spacecraft level testing. These coils were also used during instrument environmental testing and spacecraft environmental testing.

CALIBRATION RESULTS SUMMARY

To summarize the MAG calibration, this section gives the conversions that must be applied to convert the telemetered data to engineering units (nT), convert the values to an orthogonal sensor coordinate system, remove the azimuth rotation of sensor coordinates relative to spacecraft coordinates, and correct the timing latency. These conversions are for the 17-bit resolution telemetered data. One first subtracts the offsets from the signed counts:

$$c_x = c_{x-raw} - c_{x0}; \quad c_y = c_{y-raw} - c_{y0}; \quad c_z = c_{z-raw} - c_{z0}$$
$$\text{Coarse range}: (c_{x0}, c_{y0}, c_{z0}) = (-30.5, -65.2, -16.2) \tag{4}$$
$$\text{Fine range}: (c_{x0}, c_{y0}, c_{z0}) = (-1018, -2186, -544)$$

The conversion from 17-bit counts to nano-tesla is then applied:

$$b_x = k_x c_x; \quad b_y = k_y c_y; \quad b_z = k_z c_z$$
$$\text{Coarse range}: (k_x, k_y, k_z) = (1.5652,\ 1.5642,\ 1.6103) \tag{5}$$
$$\text{Fine range}: (k_x, k_y, k_z) = (1.4967,\ 1.4936,\ 1.5360)/32$$

The converted telemetry values are then converted to an orthogonal sensor coordinate system (note that this is not a coordinate transformation but an alignment correction):

$$\begin{aligned} B_{x-mag} &= b_x \\ B_{y-mag} &= \alpha b_x + b_y \\ B_{z-mag} &= \beta b_x + \gamma b_y + b_z \\ \alpha &= -0.00462; \quad \beta = +0.00053; \quad \gamma = -0.00736 \end{aligned} \tag{6}$$

Finally the magnetic field values are transformed to spacecraft coordinates using the provisional transformation matrix:

$$\begin{pmatrix} B_{x-sc} \\ B_{y-sc} \\ B_{z-sc} \end{pmatrix} = \begin{pmatrix} 1.0000 & 0 & 0.0017 \\ 0 & 1.0000 & 0 \\ -0.0017 & 0 & 1.0000 \end{pmatrix} \begin{pmatrix} B_{x-mag} \\ B_{y-mag} \\ B_{z-mag} \end{pmatrix} \tag{7}$$

Note that the diagonal elements for X and Z are $\cos(0.1^{o})$ which differ from unity only in the sixth place. The off diagonal elements between X-Y and Y-Z will be determined using the in-flight roll maneuver results described above. At this point any residual spacecraft field in spacecraft coordinates is to be removed. This residual will be determined by the in-flight calibration procedures described above but is expected to be not larger than a few nT.

Finally the MET time of the value as determined from the telemetry data, t_{TLM}, needs to be corrected for the instrument's intrinsic time latency (0.067s) and the IIR digital filter delay ($t_{IIR\text{-}lag}$) to give the magnetic field time, t_B (in seconds) with an uncertainty of 25 ms

$$t_B = t_{TLM} - 0.067s - t_{IIR-lag}(Rate) \tag{8}$$

where $t_{IIR\text{-}lag}$ depends on the science data output rate as given in Table 5.

REFERENCED DOCUMENTS

MESSENGER Magnetometer Instrument Flight Software Specification: JHU/APL 7387-9041. [MAG-IFSW]

MESSENGER Data Management and Science Analysis Plan: JHU/APL 7384-9019 [DMAP].

MAG-MESSENGER Interface Control Document: JHU/APL 7384-9223.

REFERENCES

Anderson, B. J., L. J. Zanetti, D. H. Lohr, J. Hayes, M. H. Acuna, C. T. Russell and T. Mulligan, In-flight calibration of the NEAR magnetometer, *IEEE Trans. Geoscience and Remote Sensing, 39*, 907-917, 2001.

Burlaga, L. F., Magnetic fields and plasmas in the inner heliosphere: Helios results, *Planetary and Space Sci.*, *49*, 14-15, p. 1619-1627, 2001.

Christon, S. P., A comparison of the Mercury and Earth magnetospheres: Electron measurements and substorm time scales, *Icarus*, *71*, No. 3, 448-471, 1987.

Connerney, J. E. P., Ness, N. F., Mercury's magnetic field and interior, in Mercury (F. Vilas, C. R. Chapman, and M. S. Matthews, Eds.), University of Arizona Press, Tucson, pp. 494–513, 1988.

Glassmeier, K.-H., N. P. Mager and D. Y. Klimushkin, Concerning ULF pulsations in Mercury's magnetosphere, *Geophys. Res. Lett.*, *30*, SSC 4-1, doi:10.1029/2003GL017175, 2003.

Korth, H., B. J. Anderson, M. H. Acuna, J. A. Slavin, N. A. Tsyganenko, S. C. Solomon, R. L. McNutt, Determination of the properties of Mercury's magnetic Field by the MESSENGER mission, *Planet. Space Sci.*, *54*, 733-746, 2004.

Ness, N. F., K. W. Behannon, R. P. Lepping, Y. C. Whang, Observations of Mercury's magnetic field, *Icarus 28 (4)*, 479–488, 1976.

Potter, A. E. and T. H. Morgan, Evidence for Magnetospheric Effects on the Sodium Atmosphere of Mercury, *Science*, New Series, *248*, No. 4957, pp. 835-838, 1990.

Slavin, J. A., J. C. J. Owen, J. E. P. Connerney, and S. P. Christon, Mariner 10 observations of field-aligned currents at Mercury, *Planet. Space Sci. 45 (1)*, 133–141, 1997.